Available online at www.sciencedirect.com
ScienceDirect
Journal of Colloid and Interface Science 307 (2007) 56–63
JOURNAL OF Colloid and Interface Science
www.elsevier.com/locate/jcis

Probing particle structure in waterborne pressure-sensitive adhesives with atomic force microscopy

C.H. Lei [a], K. Ouzineb [b], O. Dupont [b], J.L. Keddie [a,*]

[a] *Department of Physics, School of Electronics and Physical Sciences, University of Surrey, Guildford, Surrey GU2 7XH, UK*
[b] *Cytec Surface Specialties, Anderlecht Str. 33, B-1620 Drogenbos, Belgium*

Received 4 September 2006; accepted 20 November 2006

Available online 30 November 2006

Abstract

There is a need to know the nanostructure of pressure-sensitive adhesive (PSA) films obtained from waterborne polymer colloids so that it can be correlated with properties. Intermittent-contact atomic force microscopy (AFM) of an acrylic waterborne PSA film identifies two components, which can be attributed to the polymer and the solids in the serum (mainly surfactant). It is found that when the average AFM tapping force, F_{av}, is relatively low, the polymer particles appear to be concave. But when F_{av} is higher, the particles appear to have a convex shape. This observation is explained by a height artefact caused by differences in the indentation depths into the two components that vary with the tapping amplitude and F_{av}. To achieve the maximum contrast between the polymer and serum components, F_{av} should be set such that the indentation depths are as different as possible. Unlike what is found for the height images, the phase contrast images of the PSA do not show a reversal in contrast over the range of tapping conditions applied. The phase images are thus reliable in distinguishing the two components of the PSA according to their viscoelastic properties. At the surface of films dried at room temperature, the serum component is found in localized regions within permanent depression into the film.

Keywords: Latex; Surfactant; Atomic force microscopy; Indentation; Adhesive; Nanostructure; Film formation; Height artefacts

1. Introduction

Pressure-sensitive adhesives (PSAs) constitute a distinct category of adhesives that instantly wet and firmly adhere to a variety of dissimilar surfaces, when applied with only light pressure, without activation by water, heat or solvent [1,2]. Tighter environmental regulations [3] in the production of PSAs have led to a shift away from solvent-cast formulations to aqueous dispersions of polymer colloids, i.e., latex. Hence, waterborne PSA technology has increasingly more often been a subject of research, as demonstrated by a recent review article on the topic [4].

Generally, it has been found that the performance of waterborne acrylic PSAs is inferior to that of their solvent-based counterparts. They exhibit lower water resistance [5,6], a tendency to whiten in moist atmospheres, and lower tack, adhesion and shear strengths [7–10]. On the positive side, polymer colloids offer a facile means to tailor the structure of adhesive films at the nanometer length scale [11]. Nanostructured particles have been used to create films with remarkable mechanical properties [12]. A large body of research on *non*-colloidal (e.g., solvent-cast) copolymers in adhesives has established clear correlation between the molecular structure of films and their adhesive performance. For instance, the effects of factors such as gel content [10], molecular weight [13], and crosslinking [14] have been established. There is a much smaller body of work to correlate the molecular architecture and nanostructure of *waterborne* colloidal films with their adhesion properties [15–18]. In waterborne PSAs, the distribution and migration of small molecules, especially surfactants [7,9,19], has been correlated with poor waterborne adhesive performance and is of special interest. Greater understanding of surfactant distribution normal to the film surface has been obtained recently from modeling [20] and experiment [21]. This present work is partly motivated by

* Corresponding author. Fax: +44 1483 686781.
E-mail address: j.keddie@surrey.ac.uk (J.L. Keddie).

0021-9797/$ – see front matter
doi:10.1016/j.jcis.2006.11.036

a need for information about surfactant distribution in waterborne PSAs, which will be correlated with studies of adhesion characteristics in future work.

Transmission [22,23] and scanning electron microscopy [24,25] are well established as methods for determining the structure of individual latex particles and films. More recently, scanning near-field optical microscopy [26] has been applied for these purposes. In our previous research [27–30], we determined the morphology of waterborne PSA films using atomic force microscopy (AFM), as a first step in correlation with properties. AFM is attractive, because it offers not only topographical information but also insight into the local mechanical properties at the nanoscale. Although AFM has been used for well over a decade for studies of latex particles and films [31], there is very little work on the interpretation of images for these types of materials. The very soft particles used for PSAs, as well as the presence of latex serum solids in the dry film, present particular challenges in imaging and interpretation. Until the structure of PSA films can be determined with confidence, it will not be possible to obtain an understanding of structure–property relationships. This present work seeks to develop a reliable understanding of the nanostructure of PSA particles and films through the robust interpretation of AFM images.

A chief concern among AFM users is how to determine the "true" structure of a soft surface. In providing topographic images of soft surfaces, the technique is prone to height artefacts that can be misleading to the viewer. For several years now, it has been recognized that height images obtained with intermittent contact (also called the tapping mode) do not necessarily indicate true surface topography [32,33]. For instance, it has been shown that differences in the tip indentation depth into hard and soft phases on a smooth triblock copolymer surface create a false impression of surface topography [34]. That is, instead of representing the true surface topography, the image is a map of indentation depths.

In a different study of a triblock copolymer, reversals in the contrast in both phase and height images were observed as the tapping force and indentation depth increased [35]. This reversal was explained by a switch in the tip–sample interaction from an attractive to repulsive force for the harder phase but not for the softer phase, because of a slower tip speed and greater deformation in the latter. In related work on blends of glassy and rubbery polymers [36], two different contrast reversals were observed in both the height and phase images as the tapping force was increased. The first flip, which occurred at lower force levels, was related to a switch-over of the tip–sample interaction forces from attractive to repulsive, as in the other study. The second flip, occurring at higher force levels, however, was related to the large deformation of the matrix region.

Height artifacts and reversals in contrast have thus been well documented in diblock copolymers and polymer blends. However, they have not been reported nor explored in detail in the literature on colloidal PSA films. This gap in the literature is addressed in the present work. In the application of AFM to PSA films, a stiff cantilever and large tapping amplitude is usually applied in order to obtain reliable images [27]. Under these conditions, imaging is not performed in the attractive region at the beginning of tip–sample contact. Thus, there is a distinct difference in the conditions of imaging in comparison to what is used for polymer blends and copolymers. Herein, we report reversals in the apparent height in colloidal PSA films and show how to understand them. We explore the reliability of phase contrast images in being able to distinguish between polymer and surfactant components.

2. Materials and methods

2.1. Preparation of PSA latex

The PSA latex was synthesized by a semi-continuous emulsion polymerization process initiated by ammonium persulfate. Latex particle stability is controlled by a mixture of anionic surfactants (2 wt% on the total monomer charge). Na_2CO_3 is used as a buffer. Polymerizations were carried out in a 3-l glass reactor equipped with a reflux condensor and anchor stirrer. The temperature was controlled through the circulation of water from a thermostatic bath in the reactor jacket. The latex solids content was determined gravimetrically to be 55 wt%. The pH of the dispersion is 5.0.

The latex is made from a random copolymer of 2-ethyl hexyl acrylate (2-EHA) (glass transition temperature, $T_g = -85\,^{\circ}C$ [37]), ethyl acrylate ($T_g = -22\,^{\circ}C$ [37]), and methyl methacrylate (MMA) ($T_g = 105\,^{\circ}C$ [37]) as the main monomers. The latex polymer has a $T_g = -50\,^{\circ}C$, and an average particle diameter of 226 nm (measured with quasi-elastic light scattering (Nicomp™, 380 ZLS)). The gel fraction of the latex particles is approximately 50%, indicating some light crosslinking in the copolymer.

2.2. Film formation

Films were cast onto silicone-coated paper release liners (30 cm × 20 cm) using a 40 μm hand-held bar coater. The films were dried either in ambient conditions, or under laminar air flow for 3 min on heated plates at 110 °C. The dried films for AFM analysis were about 20 μm thick.

2.3. Atomic force microscopy

Small pieces (1 cm × 1 cm) of the cast PSA were cut from the large-area films and were analyzed with an atomic force microscope (NTEGRA, NT-MDT, Moscow, Russia) within 24 h of casting. All scans were carried out with intermittent contact between the AFM tip and the film surface. All scans used a silicon cantilever (ATEC-NC, Nanosensors, Switzerland) equipped with an ultrasharp, conical silicon tip having a radius of curvature less than 10 nm. The nominal resonant frequency f_0 of the cantilever is about 330 kHz and its spring constant k is about 45 N/m.

AFM analysis was performed on the original interface with air. Images were recorded simultaneously in the topographic (height) mode and in the phase mode, with scan sizes ranging from 5 to 30 μm. The optimum method for obtaining images

of latex PSA surfaces has been reported previously [27]. Parameters needed to describe the tapping conditions are the "free" amplitude A_0 (corresponding to oscillation in air) and the setpoint amplitude A_{sp} (corresponding to the amplitude when the tip is in contact with the sample surface).

The potential energy of vibration for a cantilever is given as $0.5kA_0^2$. Thus, the larger the values of k and A_0, the higher is the vibration energy. The high tack of the PSA surface makes it necessary to use high k and A_0 to impart enough energy to the tip to "pull off" of the adhesive surface. To obtain values of A_0 and A_{sp} in metric units, a systematic calibration of the cantilever was obtained from amplitude–distance curves on a clean silicon wafer, assuming no deformation of the silicon surface and no bending of the cantilever during tapping [38].

It is, however, important to realize that, in all cases, the AFM tip does indent to a depth z_{ind} into the soft PSA surface [27]. When the tip of an oscillating cantilever with a setpoint amplitude of A_{sp} is in contact with a soft PSA surface, the distance between the tip and sample, d_{sp}, is always less than A_{sp}. Then, z_{ind} is found from the difference between these two values:

$$z_{ind} = A_{sp} - d_{sp}. \tag{1}$$

This relationship between the three parameters is illustrated in Fig. 1.

All AFM images presented here were obtained with very similar tapping conditions. Typically, A_0 was 290 nm, and d_{sp} was between 150 and 250 nm for all measurements. This relatively high A_0 was used in this analysis in order to impart tip stability (i.e., the widest range of acceptable A_{sp} values) and to increase the average tapping force, F_{av}, to reveal subsurface structure. These tapping conditions also ensure that the indentation of the AFM tip into the PSA surface is small enough to avoid significant distortion of the morphology [27].

3. Results and discussion

3.1. Initial study of film structure

We start the discussion by considering the physical significance of the tapping parameters. A freely oscillating cantilever has a resonant frequency f_0, where the tapping amplitude will be at a maximum value of $A_0(f_0)$. Imaging is performed at a frequency f set slightly lower than f_0 such that $A_0(f)$ is typically 5% less than the peak value at $A_0(f_0)$. The lower that the setpoint tapping amplitude A_{sp} is, in comparison to A_0, the greater is F_{av}. This important parameter is given in a semi-empirical equation as [39]

$$F_{av} = \frac{1}{2}\frac{k}{Q}\left[1 - \frac{A_{sp}}{A_0(f_0)}\right]A_0(f)\beta, \tag{2}$$

with the off-resonance parameter β given as

$$\beta = \frac{A_0(f)}{A_0(f_0)} \tag{3}$$

and where Q is the quality factor of the cantilever. Following from the above statements, $\beta < 1$ in all cases. Note the importance of the *ratio* of A_{sp} to A_0 in determining F_{av}, rather than the individual value of A_{sp} alone. Su et al. have measured F_{av} systematically as a function of A_0 and A_{sp}/A_0 [40]. For a particular AFM tip, Q is obtained from the ratio of f_0 to the full bandwidth at 0.707 of the maximum amplitude, Δf [41]:

$$Q = \frac{f_0}{\Delta f}. \tag{4}$$

The cantilever used in our analysis has a Q value that was determined experimentally to be 690. We have estimated F_{av} in our experiments using Eqs. (2) and (3).

In the intermittent contact (or tapping) mode of operation, a phase image can be obtained simultaneously with the height image. The phase image presents the phase lag, ϕ, of the photodiode output signal in relation to the driving piezoelectric signal as a function of position within the scan area. Changes in ϕ reflect variations in the energy dissipation, E_D, of the cantilever as its tip moves laterally across a surface. ϕ is related mathematically to E_D as [42,43]

$$\sin\phi = \left(\frac{f}{f_0}\frac{A_{sp}}{A_0}\right) + \frac{QE_D}{\pi k A_{sp} A_0}, \tag{5}$$

where all the variables are as already defined. During a scan, all of the parameters in Eq. (5) except E_D are fixed, so the phase image provides a map of E_D [43]. When the tip interacts with a highly viscous region on a surface, or a viscoelastic region in which the viscous component is high, more energy will be dissipated, and therefore E_D and ϕ will be greater. When the tip interacts with a viscoelastic region in which the elastic component is higher, however, it is expected that less energy will be dissipated, making ϕ smaller [44]. In the phase contrast images presented in this work, lighter areas correspond to lower values of ϕ, and darker areas correspond to larger values. Hence, in phase contrast images, more energy dissipative regions will appear darker.

Fig. 2 shows images of the same latex film surface using two different setpoint ratios. In Fig. 2a, a relatively high A_{sp}/A_0 ratio was used, such that F_{av} is low (1.3 nN), whereas Fig. 2b is the result of a relatively low A_{sp}/A_0 ratio, such that F_{av} is high (4.4 nN). Clear particle identities are observed in the images. In both the height and the phase images, there is no evidence for particle coalescence. In the height images, it is notable that particles appear to be concave under a low F_{av} but convex under the higher F_{av}. This result is discussed in detail later in this paper.

In the phase images, there is strong contrast between the particles and the component surrounding them. Other experiments

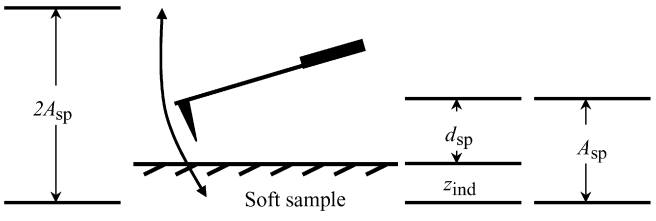

Fig. 1. Schematic illustration showing that the setpoint amplitude A_{sp} is equal to the sum of the tip–sample distance d_{sp} and the indentation depth z_{ind}.

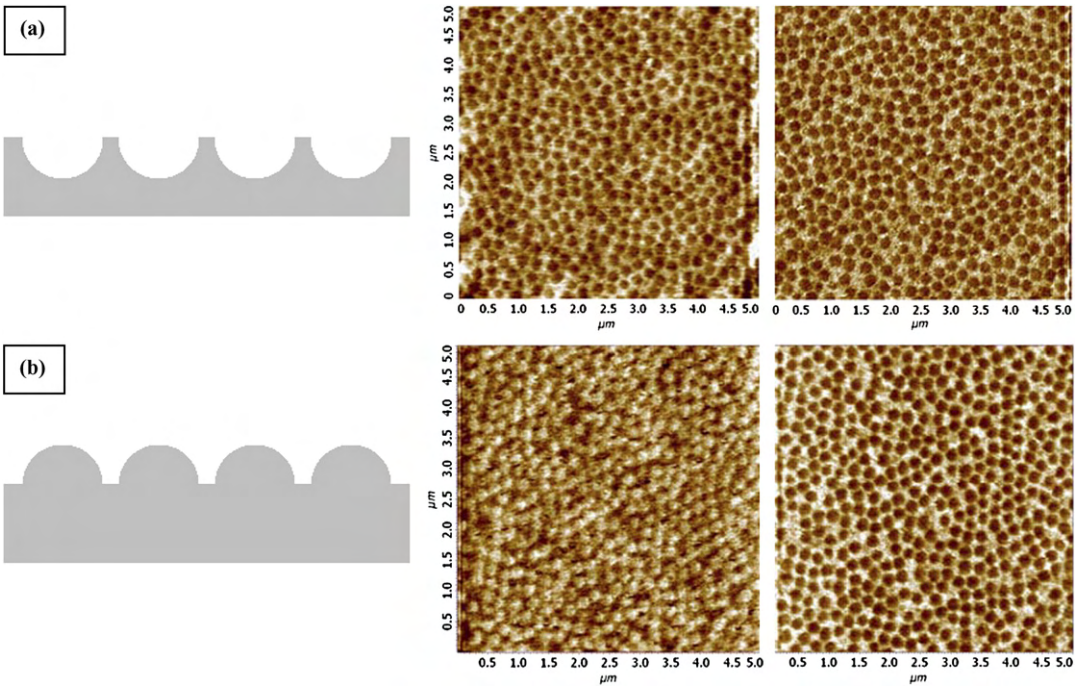

Fig. 2. AFM images (topographic on left; phase on right) of a 20 μm latex film (dried at 110 °C) obtained using A_0 set at 290 nm (a) with $A_{sp} = 244$ nm ($F_{av} = 1.3$ nN) and (b) $A_{sp} = 139$ nm ($F_{av} = 4.4$ nN). All images are 5 μm × 5 μm. On the right side, the apparent surface structure (concave in (a) and convex in (b)) is shown schematically in a side view.

and modeling [44] has shown that contrast is accentuated in phase images when there is a low A_{sp} and a high A_0, as is the case here. For either value of A_{sp}, the phase images indicate that there is greater energy dissipation when the tip interacts with the polymer particles in comparison to the region surrounding the particles. We attribute this phase contrast to the effect of having two components with differing viscoelastic properties. The images show that the tip is dissipating more energy when interacting with the polymer particles.

The reasons for contrast in phase images has been a subject of frequent investigation [33,34,43–45]. Phase contrast has been shown to be independent of variations in the elastic moduli (i.e., stiffness) of polymers [46,47], because the energy used in surface deformation is elastically recovered. One exception is when the elastic modulus of a region is very low. In this case, the AFM tip will push deeper into the surface and thus have a greater contact area with the deformed surface. The interaction energy will then be greater [43]. On the other hand, when the tip interacts with a viscous material, energy is dissipated. There is convincing evidence from experiments and modeling [43,48] that the energy dissipation in tip–sample interactions is greater in viscoelastic materials with a high viscosity. Variations in viscosity across a surface therefore lead to contrast in phase images and have indeed been observed over lateral distances of a few nm [48].

Equation (5) shows that ϕ is affected by the tapping conditions (A_0 and A_{sp}) and also by the cantilever choice (k and Q). However, the images in Fig. 2 reveal that the *contrast* between the components in the phase image is not strongly affected by A_{sp}, whereas the height image is strongly affected. Furthermore, there is *not* a reversal in the contrast of the phase image, whereas a reversal from concave to convex is seen in the height image.

Unlike what is seen in our results, the contrast in both height and phase images has been found elsewhere [33,36,44,49] to *reverse* in regimes where there is either a very low or a very high A_{sp}. Because in this present work a large F_{av} is used (produced by a relatively high A_0 and low A_{sp}), the bi-stable regime for ϕ, reported elsewhere [42], is avoided. Likewise, the attractive regime at very low A_{sp} is avoided. Hence, the chosen conditions of tapping avoid artefacts in the phase images and make the images relatively insensitive to variations of A_{sp} within the ideal region.

To understand better the influence of F_{av} on apparent film and particle structure, an image of the latex surface was obtained with a fixed A_0 but with A_{sp} varying in small increments during an AFM scan. Fig. 3 shows that the apparent particle structure switches from convex to concave with increasing A_{sp} (and decreasing F_{av}). With the lower A_{sp}, the topographical contrast between the particles and the surrounding region is low. The phase image remains essentially unchanged as A_{sp} is varied in this range.

The question arises as to what is the true structure of the adhesive surface. Depending on F_{av} (as adjusted through A_{sp}), one can conclude that particles are protruding up from a surface or sunk beneath the surface. Further investigation was therefore required to interpret the images. Our approach was to isolate the components of the latex so that their interactions with the AFM tip could be studied independently.

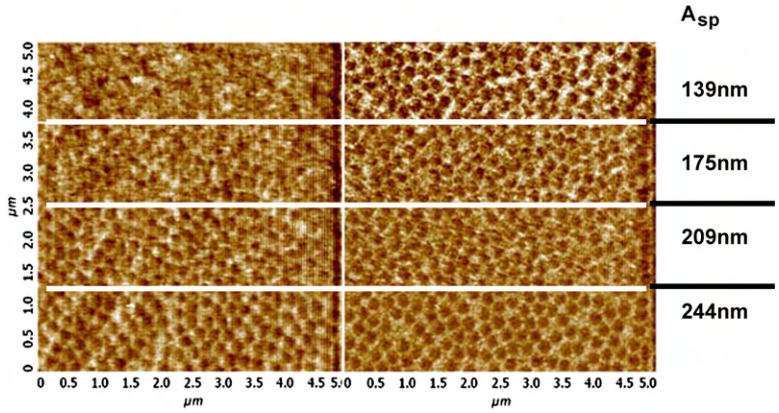

Fig. 3. AFM images obtained with $A_0 = 290$ nm. A_{sp} is increased from the top to bottom as indicated. Image size is 5 μm × 5 μm.

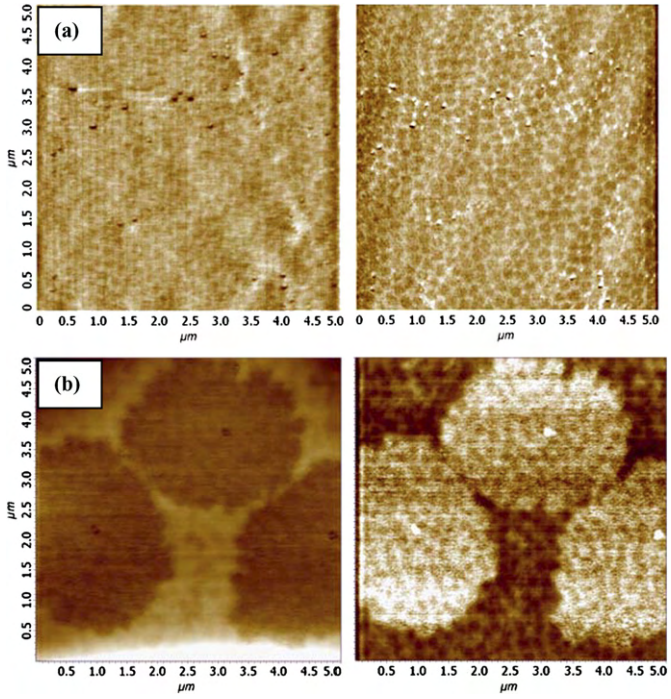

Fig. 4. AFM images (topographic on left; phase on right) of 20 μm thick latex films dried at room temperature, obtained using $A_0 = 290$ nm and $A_{sp} = 244$ nm. (a) Film from dialyzed latex; (b) film from as-prepared latex, dried at room temperature. Image sizes are 10 μm × 10 μm.

3.2. Separate imaging of surfactant and polymer components

The brighter regions in the phase images, in which less energy is dissipated when the tip interacts with the surface, are presumed to be the serum solids (mainly surfactant). For the purposes of fundamental study, the polymer phase was isolated from the serum phase through dialysis. Films cast from the dialyzed latex are presumed to consist primarily of the acrylic polymer. Fig. 4a shows the structure that was identified with AFM. The particle identity is poorly defined compared to that in the as-prepared latex (shown previously in Fig. 2). The phase image shows that a large fraction of the surface consists of a single material. There are some regions around the particles that suggest the presence of some residual serum phase, but these regions are not clearly defined.

It was discovered that if a latex film was dried at room temperature (21 °C), island-like regions that were more than 1 μm across appeared at the film surface. Fig. 4b shows the typical structure. From the height image, it is apparent that the particle identity is not as clearly defined as in the latex dried at high temperature (cf. Fig. 1). It is likely that the film surface is covered more by the serum (surfactant) component so that the particles are not apparent. In the phase image, there is very strong contrast between these island-like regions and the surrounding region. It was speculated that the island-like regions consist of the surplus serum solids. Further experiments were conducted to determine the water solubility of these regions as a means of confirming whether they consist of the serum phase.

Films that had been dried at room temperature were submerged into water for 30 min and then rinsed with flowing water for several minutes. Fig. 5 compares the observed structures before and after rinsing. The "islands" that had been observed in the phase images of the as-prepared latex disappeared after rinsing. In the height images, however, the islands appear as depressions both before and after rinsing. This experiment indicates that the material in the island structure is water-soluble. It is therefore highly likely to be the serum solids, mainly surfactant. There is a permanent depression in the sample surface associated with the islands. Further experiments were carried out to ascertain the true particle structure (whether concave or convex) and whether the island structures are truly in depressions in the surface.

3.3. The effect of A_{sp} on image contrast

Amplitude–distance (A–z) curves for hard surfaces have been thoroughly discussed elsewhere [50] as a means of studying interactions between AFM tips and sample surfaces. For a hard surface, as the distance between the tip and surface, z, is reduced at a fixed A_0, there will be a corresponding and *equal* decrease in A. For a soft surface, on the other hand, A will not decrease as much as z as the tip approaches the sample because of tip indentation into the surface.

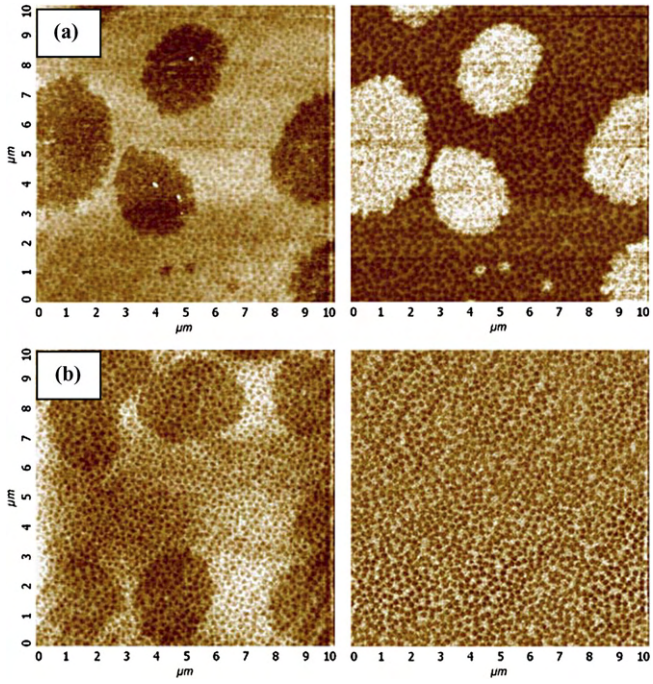

Fig. 5. AFM images (topographic on left; phase on right) of as-prepared latex films dried at room temperature (a) before soaking/rinsing with water and (b) after soaking in water for 30 min and rinsing.

A–z analysis was conducted on the two isolated components of the latex films (serum and polymer) as a way to explain and interpret the images presented in Figs. 2 and 3. Typical A–z curves from the polymer phase (obtained from the dialyzed latex) and from the serum phase (obtained from the island region on an as-prepared RT dried latex) are compared in Fig. 6. The A–z curve from the dialyzed latex (almost pure polymer component) is regarded as equivalent to the center of the latex particles in Figs. 2 and 3. On the other hand, the A–z curve from the island region on an as-prepared RT dried latex (rich in the serum solids) is regarded as equivalent to the serum component surrounding the particles in Figs. 2 and 3. On the right-hand side of Fig. 6 are two height images obtained from a latex film dried at 110 °C, using a setpoint $A_{sp} = 139$ nm and a setpoint $A_{sp} = 244$ nm, which are matched with the corresponding point in the A–z curves. For a given z, the difference in A between the hard silicon surface and the polymer surface is equal to z_{ind}.

In the scans presented in Fig. 3, the particles appear to be convex when $A_{sp} = 139$ nm and concave when $A_{sp} = 209$ nm, while at $A_{sp} = 175$ nm, there is very low contrast between the two components so particle identity is not very clear. The crossover of the A–z curves in Fig. 6 at $z = 180$ nm is consistent with the low contrast in the images obtained in the same region ($A_{sp} = 175$ nm in Fig. 3). The amplitude at the crossover point corresponds to $F_{av} = 3.2$ nN.

Through the quantitative comparison of the A–z curves for the two components to what is obtained from silicon, a mea-

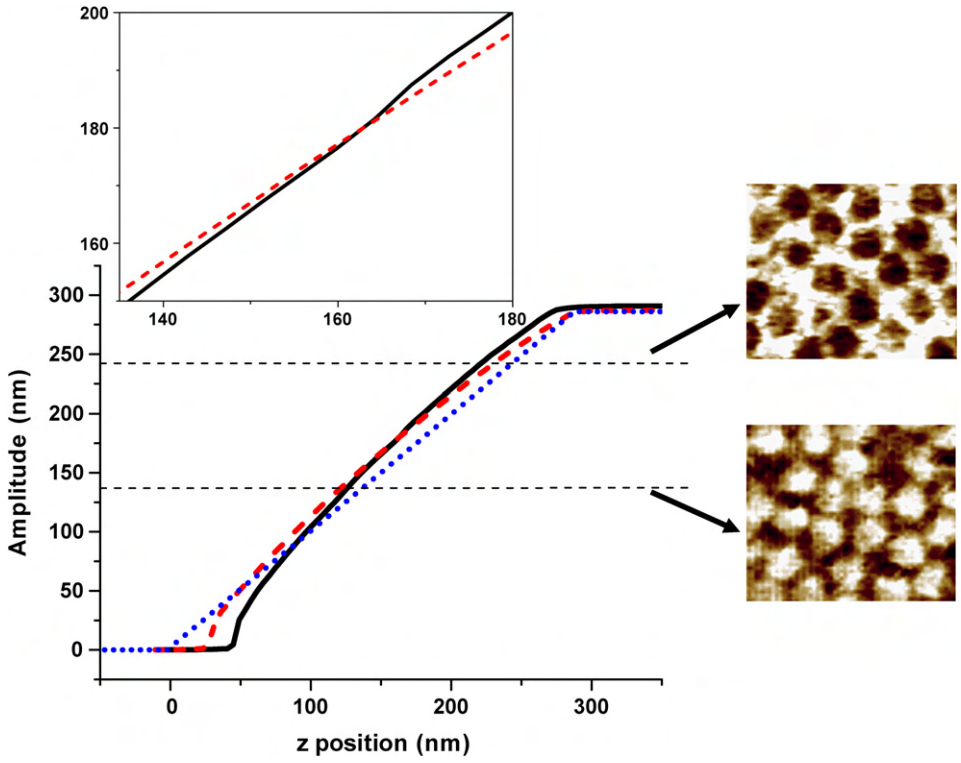

Fig. 6. Measurements of tip vibration amplitude A as a function of z for two different latex components: polymer surface (solid curve) obtained from a RT-dried dialyzed latex and the serum phase (dashed curve) obtained from the island on a RT- dried latex film. The dotted curve was obtained from a Si wafer surface. The inset shows the crossover point of the solid and dashed curves. On the right-hand side are two height images obtained from a latex film dried at 110 °C, using a low setpoint ($A_{sp} = 139$ nm) and a high setpoint ($A_{sp} = 244$ nm).

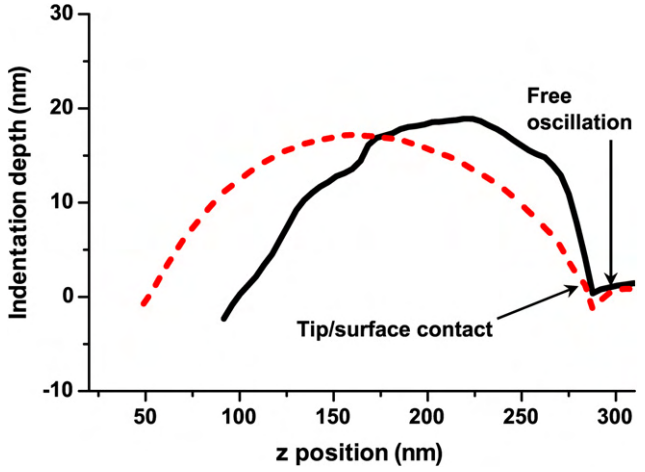

Fig. 7. Tip indentation depth as a function of z for the two different latex components: dialyzed polymer (solid curve) and the serum solids (dash curve). A_0 is 280 nm, and contact is made with the sample surface at this value of z.

sure of the indentation depths is obtained (Fig. 7). As the tip approaches the surface, z_{ind} first increases as the tip digs deeper into the surface, and it then reaches a maximum value. Thereafter, as the tip is drawn closer, the apparent z_{ind} falls to zero, because the cantilever is not energetic enough to pull off of the adhesive surface and it is unstable. As expected from Fig. 6, there is a crossover point between the indentation curves for the two components. Above the crossover point (at higher A_{sp}), the polymer particles are more indented compared to the serum solids and they therefore appear concave. Below the crossover point (at lower A_{sp}), the polymer particles are indented less than the serum component, and the particles appear convex. Analysis of the indentation depths indicates that when $A_{sp} = 139$ nm, z_{ind} is 11 nm for the polymer and 16 nm for the serum solids. At $A_{sp} = 244$ nm, z_{ind} is 22 nm for the polymer and 13 nm for the serum solids. These differences in z_{ind} explain why the same surface in Fig. 6 is seen to have both a convex and concave structure, depending on the tapping conditions.

Finally, we note that in Figs. 4b and 5a, the height image presents the surfactant islands as being *lower* than the plane of the film surface. It is concluded that there are depressions in the film that are filled with the serum phase.

4. Conclusions

Analysis of A–z curves for polymer and serum components in PSA films has revealed that when the average AFM tapping force, F_{av}, is relatively low, the indentation depth in the polymer is greater than in the serum solids. Hence in this particular PSA, the polymer particles appear concave. But when F_{av} is higher, the opposite is true, and the particles appear to be convex. The crossover point occurs at $A_{sp} = 180$ nm, which corresponds to $F_{av} = 3.2$ nN. The phase images, on the other hand, are much less sensitive to the tapping conditions and do not undergo a reversal in contrast when F_{av} is varied. They can be reliably used to distinguish the components of the PSA by differing viscoelasticity.

There are distinct differences in our findings for AFM imaging of PSA films and what has been reported in the literature for copolymers and polymer blends. In PSA films, there is a reversal in the height but *not* in the phase contrast. In AFM analysis of these other polymer systems, reversals are reported in both height and phase images. In the latter case, contrast reversals occur when moving from the attractive to repulsive regions of tip–sample interaction. In our imaging of PSA films, high tapping forces are used, and the analysis is not conducted in the attractive regime. Therefore there is a different reason for the contrast reversal of height images of PSA films, related to differences in the indentation depths of the materials components, as was determined herein.

At the surface of films dried at room temperature, the serum solids are found in localized regions, or islands. When the serum solids are removed through rinsing with water, there is a permanent depression in the film. The reasons for the heterogeneity of the serum solids at the PSA surface will be explained in a future publication.

Acknowledgments

We benefited from technical assistance and advice from P. Zhdan (University of Surrey) and S. Nesterov (NT-MDT). Funding for this work was provided by the European Commission's Framework 6 Programme (NsHAPe project, Contract No. 505442). We appreciate useful discussions with P.A. Lovell (University of Manchester), C. Creton (ESPCI) and A.F. Routh (University of Cambridge).

References

[1] C. Creton, MRS Bull. 28 (2003) 434.
[2] D. Satas, Handbook of Pressure Sensitive Adhesives, third ed., Van Nostrand–Reinhold, New York, 1989.
[3] H. Jotischky, Surf. Coat. Int. 84 (2001) 11.
[4] R. Jovanovic, M.A. Dube, J. Macromol. Sci. Polym. Rev. C 44 (2004) 1.
[5] J. Mulvihill, A. Toussaint, M. De Wilde, Prog. Org. Coat. 30 (1997) 127.
[6] E. Aramendia, M.J. Barandiaran, J. Grade, T. Blease, J.M. Asua, Langmuir 21 (2005) 1428.
[7] J.Y. Charmeau, P.A. Gerin, L. Vovelle, R. Schirrer, Y. Holl, J. Adhes. Sci. Technol. 13 (1999) 203.
[8] A. Zosel, B. Schuler, J. Adhes. 70 (1999) 179.
[9] P.A. Gerin, Y. Grohens, R. Schirrer, Y. Holl, J. Adhes. Sci. Technol. 13 (1999) 217.
[10] S.D. Tobing, A. Klein, J. Appl. Polym. Sci. 79 (2001) 2230.
[11] J. Garrett, P.A. Lovell, A.J. Shea, R.D. Viney, Macromol. Symp. 151 (2000) 487.
[12] F.D. Dos Santos, L. Leibler, J. Polym. Sci. Part B Polym. Phys. 41 (2003) 224.
[13] H. Lakrout, C. Creton, D.C. Ahn, K.R. Shull, Macromolecules 34 (2001) 7448.
[14] A. Lindner, B. Lestriez, S. Mariot, C. Creton, T. Maevis, B. Luhmann, R. Brummer, J. Adhes. 82 (2006) 267.
[15] A. Aymonier, E. Papon, G. Castelein, A. Brogly, P. Tordjeman, J. Colloid Interface Sci. 268 (2003) 341.
[16] M. do Amaral, A. Roos, J.M. Asua, C. Creton, J. Colloid Interface Sci. 281 (2005) 325.
[17] S. Tobing, A. Klein, L.H. Sperling, B. Petrasko, J. App. Polym. Sci. 81 (2001) 2109.

[18] S.D. Tobing, A. Klein, J. App. Polym. Sci. 79 (2001) 2558.
[19] J.Y. Charmeau, R. Berthet, C. Grigreau, Y. Holl, E. Kientz, Int. J. Adhes. Adhes. 17 (1997) 169.
[20] V.R. Gundabala, W.B. Zimmerman, A.F. Routh, Langmuir 20 (2004) 8721.
[21] W.P. Lee, V.R. Gundabala, B.S. Akpa, M.L. Johns, C. Jeynes, A.F. Routh, Langmuir 22 (2006) 5314.
[22] Y. Wang, A. Kats, D. Juhue, M.A. Winnik, R.R. Shivers, C.J. Dinsdale, Langmuir 8 (1992) 1435.
[23] M. Joanicot, K. Wong, J. Richard, J. Maquet, B. Cabane, Macromolecules 26 (1993) 3168.
[24] A.M. Donald, C.B. He, C.P. Royall, M. Sferrazza, N.A. Stelmashenko, B.L. Thiel, Colloids Surf. A 174 (2000) 37.
[25] J.L. Keddie, P. Meredith, R.A.L. Jones, A.M. Donald, Macromolecules 28 (1995) 2673.
[26] É Teixeira-Neto, G. Kaupp, F. Galembeck, Colloids Surf. A 243 (2004) 79.
[27] J. Mallégol, O. Dupont, J.L. Keddie, Langmuir 17 (2001) 7022.
[28] J. Mallégol, J.-P. Gorce, O. Dupont, C. Jeynes, P.J. McDonald, J.L. Keddie, Langmuir 18 (2002) 4478.
[29] J. Mallégol, O. Dupont, J.L. Keddie, J. Adhes. Sci. Technol. 17 (2000) 243.
[30] J. Mallégol, G. Bennett, O. Dupont, P.J. McDonald, J.L. Keddie, J. Adhes. 82 (2006) 217.
[31] Y. Wang, D. Juhúe, M.A. Winnik, O.M. Leung, M.C. Goh, Langmuir 8 (1992) 760.
[32] A. Knoll, R. Magerle, G. Krausch, Macromolecules 34 (2001) 4159.
[33] J.P. Pickering, G.J. Vancso, Polym. Bull. 40 (1998) 549.
[34] S. Kopp-Marsandon, Ph. Leclère, F. Dubourg, R. Lazzaroni, J.P. Aimé, Langmuir 16 (2000) 8432.
[35] Y. Wang, R. Song, Y. Li, J. Shen, Surf. Sci. 530 (2003) 136.
[36] D. Raghavan, M. VanLandingham, X. Gu, T. Nguyen, Langmuir 16 (2000) 9448.
[37] P.A. Lovell, M.S. El-Aasser, Emulsion Polymerization and Emulsion Polymers, Wiley, Chichester, 1997.
[38] X. Chen, M.C. Davies, C.J. Roberts, S.J.B. Tendler, P.M. Williams, J. Davies, A.C. Dawkes, J.C. Edwards, Ultramicroscopy 75 (1998) 171.
[39] M.F. Yu, T. Kowalewski, R.S. Ruoff, Phys. Rev. Lett. 85 (2000) 1456.
[40] C. Su, L. Huang, K. Kjoller, Ultramicroscopy 100 (2004) 233.
[41] D. Sarid, Scanning Force Microscopy, Oxford Univ. Press, New York, 1994.
[42] P.J. James, M. Antognozzi, J. Tamayo, T.J. McMaster, J.M. Newton, M.J. Miles, Langmuir 17 (2001) 349.
[43] B. Anczykowski, B. Gotsmann, H. Fuchs, J.P. Cleveland, V.B. Elings, Appl. Surf. Sci. 140 (1999) 376.
[44] W.W. Scott, B. Bhushan, Ultramicroscopy 97 (2003) 151.
[45] R. García, R. Pérez, Surf. Sci. Rep. 47 (2002) 197.
[46] G. Bar, L. Delineau, R. Brandsch, M. Bruch, Appl. Phys. Lett. 75 (1999) 4198.
[47] J. Tamayo, R. Garcia, Appl. Phys. Lett. 71 (1997) 2394.
[48] Ph. Leclère, F. Dubourg, S. Kopp-Marsaudon, J.L. Brédas, R. Lazzaroni, J.P. Aimé, Appl. Surf. Sci. 188 (2002) 524.
[49] X. Han, J. Xu, H.L. Liu, Y. Hu, Chin. J. Chem. 24 (2006) 149.
[50] B. Anczykowski, D. Krüger, H. Fuchs, Phys. Rev. B 53 (1996) 15485.